2022

Effect of Joint Rotation on Curling Responses in Airfield Rigid Pavements

Jaime Hernandez
Marquette University, jaime.hernandez@marquette.edu

Imad L. Al-Qadi
University of Illinois - Urbana-Champaign

International Journal of Pavement Engineering, Vol. 23, No. 6 (2022): 1832-1839. DOI.

Effect of Joint Rotation on Curling Responses in Airfield Rigid Pavements

Jaime Hernadez
Department of Civil, Construction, and Environmental Engineering, Marquette University, Milwaukee, WI
Imad L. Al-Qadi
Department of Civil and Environmental Engineering, University of Illinois at Urbana-Champaign, Urbana, IL

ABSTRACT

This paper quantifies the relevance of restriction to joint rotation of an airfield concrete pavement when calculating critical curling stresses and deflections using a validated finite element model. The validation uses strains measured at the John F. Kennedy International Airport. To calculate critical curling stresses and deflections, the pavement was subjected to 5263 h of temperature variation determined by utilising the enhanced integrated climate model and thermocouple readings. The profiles include a wide range of average temperatures, temperature gradients, and temperature nonlinearity. Three conditions were included: (1) joints free to displace and rotate; (2) joints free to rotate, but partially restrained to vertical displacement; and (3)

joints partially restrained to vertical displacement and rotation. Differences in critical stresses between the second and third conditions were greater than 5% for 70% of the time. When considering rotational restriction, critical deflections are reduced. Eighty percent of the difference, with respect to the free case, was caused by rotational restriction. It was evident that joint rotation intensifies the influence of curling stresses and deflections on long-term performance of airfield rigid pavement.

KEYWORDS:

Rigid pavement, nonlinear temperature, curling stresses, partial restraint, Westergaard solutions

Introduction

Curling stresses are a consequence of temperature variation in concrete pavements. Curling stresses do not control design, but their daily and seasonal variations influence long-term performance. Westergaard pioneered the curling stresses research and developed mechanistic closed-form solutions (Westergaard 1927). Despite applied simplifications, such as infinite slab, Winkler foundation, and full contact between the slab and subbase, Westergaard's solutions remain relevant.

The accuracy of Westergaard's solutions have been enhanced over the past 90 years by eliminating a few assumptions, including linear temperature distribution through the slab. Linear temperature profiles provided lower curling stresses during the evening and early morning hours and measured slab temperatures showed nonlinear profiles (Richardson and Armaghani 1987). In addition, the difference in tensile stresses between the linear and nonlinear assumption was as high as 300% (Mohamed and Hansen 1997). Ioannides and Khazanovich (1998) highlighted the relevance of self-equilibrating stresses, which are a result from the nonlinear component of the temperature profile. Hiller and Roesler (2010) reported inaccurate pavement fatigue life predictions when omitting temperature nonlinearity.

In addition to temperature, curling stresses depend on the Portland cement concrete (PCC) properties, slab geometry, supporting structure (i.e. subbase and subgrade), and connectivity among slabs (Ceylan *et al.* 2016). However, limited work has been done on slab connectivity effects on curling responses.

Some efforts modelled concrete pavement and dowel bars using finite elements. Deflections predicted from the finite-element model (FEM) were smaller than those calculated using Westergaard's equations, when assuming a linear temperature gradient (William and Shoukry 2001). The FEM calculated stresses were 9.3% and 16% greater than those calculated by Westergaard equations for the centre and joint, respectively. These differences were smaller when 24-degrees-of-freedom brick elements were used in the FEM (Shoukry *et al.* 2007).

To reduce the computation cost and investigate the insensitivity of curling stresses to shear springs, dowel bars were modelled as linear springs (Nishizawa *et al.* 1996). Rotational springs caused difference in the curling stresses up to 8% when the temperature gradient was 16.1°C. The curling stress differences increased for stiffer rotational springs. Because the difference was relatively small, proposed equation for curling stresses overlooked the spring bending. Close-form solutions for partially restrained slab-on-grade PCC pavement and pavement blowup have been proposed by Hernandez and Al-Qadi (2018, 2019 respectively).

In this study, the researchers evaluated the combined effect of a nonlinear temperature profile and slab connectivity on curling stresses and deflections using a validated FEM. Tensile stresses and corner deflections due to temperature, which are superimposed to load-related stresses and affect fatigue life and faulting, were used to evaluate the effect of the mentioned factors. Experimental measurements have shown that curling remains mostly upward during the life of a pavement (Asbahan and Vandenbossche 2011). Consequently, once curling stresses are added to load-related stresses, calculations of top-down fatigue cracking can be greatly

affected by including the degree of restriction along the edges of the concrete pavement. Measured temperature and a modified version of the enhanced integrated climate model (EICM) were used to predict temperature profiles. The temperature input covered 5,263 hrs and a wide range of average temperatures, temperature gradients, and degrees of nonlinearity. Linear springs in the shear and bending directions were used to simulate slab connectivity. Measured strains at the bottom of the slab were used to validate the FEM predicted strains.

Finite-element model

A rigid pavement section at the John F. Kennedy (JFK) International Airport was instrumented with pressure cells, strain gauges, and thermocouples (Garg *et al.* 2013). The pavement is composed of four layers, including: 500-mm PCC slab, 100-mm plant-mix macadam, 150-mm dense-graded aggregate base (DGAB), and subgrade. Materials were assumed linear elastic; hence, the elastic moduli of the PCC, macadam, DGAB, and subgrades were 38,852; 2000; 300; and 30 MPa, respectively. The Federal Aviation Administration (FAA) provided the values based on laboratory testing and typical values from other airfield pavement sections. The coefficient of thermal expansion of the PCC is assumed 9.0×10^{-6} mm/mm/°C (Huang 2004). The material properties are summarised in Table 1.

Table 1. Material properties in pavement structure.

Material	Thickness (mm)	Elastic Modulus (MPa)	Poisson's Ratio
Concrete	500	38852	0.15
Macadam	100	2000	0.35
DGAM	150	300	0.30
Subgrade	–	30	0.40

The FEM was developed using the general-purpose finite-element software ABAQUS. Special features regarding mesh, interaction between layers, and slab connectivity were considered in the 3D FEM (see Figure 1). The 7.6-m square PCC slab was meshed with four-node shell elements. The macadam and DGAB extended to infinity in the xz-plane. These layers were meshed with two types of elements – eight-node linear brick and infinite elements on the boundaries. The subgrade extended to infinity along the three perpendicular directions.

Figure 1. Three-dimensional finite-element model in ABAQUS finite element model, with detail of the boundary conditions.

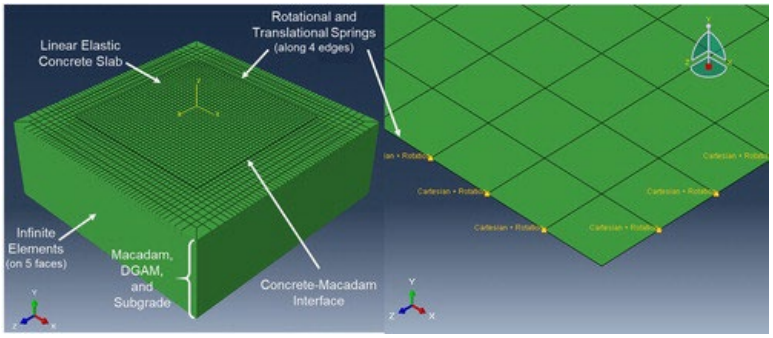

The interaction between concrete and its underlying layer was defined using the penalty formulation along the tangential direction with a friction coefficient of 1.5. The penalty method is enforced with stiffness and allows relative displacement between the contacting surfaces. The penalty formulation does not include a shear stress limit. For the same interface, contact in the normal direction allows separation while it prevents penetration

from one surface to the other. The other interactions were defined in a similar fashion but using a friction coefficient of 1.0 instead of 1.5. Separation is prevented for Macadam-DGAM and DGAM-subgrade interfaces as it is an appropriate representation because the layers do not curl as concrete slab does (Huang 2004; Yoo *et al.* 2006).

Finally, elastic rotational and translational springs connected the PCC slab to the surrounding media. The springs' magnitude controlled the transfer of displacement and rotation among slabs. For instance, translational springs with large magnitude represent full transfer of vertical displacement; however, if vertical displacement does not transfer from one slab to another, the constant of the vertical spring is zero. Similar reasoning can be applied to rotational springs and slab's bending. The dowel bars that connect pavement slabs behave as beams. Consequently, due to temperature, the dowels displace vertically and rotate. This would affect the curling responses. Connector elements were used to simulate rotational and translation springs. Connector elements allow to input proportionality constant between deformation (either translation or rotation) and load (force or moment). Spring stiffness is of the same order of magnitude – 10 kN/mm for translation and 10^7 kN/mm/rad for rotation – as the normalised rotational and translational restraint parameters equal to unity ($R_a = R_b = T_a = T_b = 1$ as showed in Hernandez and Al-Qadi 2018).

Mesh sensitivity analysis

The model includes four types of finite elements: CIN3D8, C3D8, C3D8R, S4 according to ABAQUS' nomenclature. S4 is a 4-node general-purpose shell, finite membrane strains and it was applied to the concrete slab. CIN3D8 is a one-way infinite three-dimensional solid continuum element with 8 nodes and it was applied to the boundaries of the model, including the bottom of the subgrade, to simulate the semi-infinite layer underneath the concrete slab. C3D8 is an 8-node three-dimensional full integration element, which was applied in the Macadam and the DGAM. Finally, the subgrade was modelled using 8-node three-dimensional elements with reduced integration.

Variation of longitudinal and transverse stresses through the slab's depth determine the optimal size of shell elements. Five mesh configurations with 9, 27, 81, 243, and 486 elements along the edge were considered; these are equivalent to 81, 729, 6561, 59,049, and 236,196 finite elements in the slab. Arrays storing the stresses at 11 section points through the slab's centre, edge, and corner were compared using the finest mesh as a benchmark. Elements smaller than 281 mm were deemed appropriate through analysis, so a 200-mm element size was selected.

Temperature profiles

Observations of temperature profiles in rigid pavements has shown that cubic regression better resembles temperature profile (Solaimanian and Kennedy 1993). Hence, at least four thermocouples distributed across the slab thickness are needed. Results from the three thermocouples, installed at the bottom half of the slab, were insufficient to develop a quadratic regression of the temperature distribution with depth. To overcome this challenge, ILLI-TERM, which provides accurate representation of temperature profile, was used and calibrated. ILLI-TERM is a modified version of the EICM; EICM is a one-dimensional model simulates heat and moisture flow within pavement structures. It is currently used by the *Mechanistic-Empirical Pavement Design Guide* to incorporate climate and environment in the calculation of stresses and deflections (AASHTO 2020). The main components of EICM are the climate–materials–structural model, frost-heave and settlement model, and the infiltration–drainage model (Lytton *et al.* 1993). One of the most recent implementations of EICM is the software ILLI-THERM (Sen and Roesler 2018). ILLI-THERM works on the same algorithms as EICM, but it excludes the infiltration–drainage model. In addition, ILLI-THERM requires multiple user inputs (e.g. thermal conductivity, heat capacity, porosity) and requires calibration to produce realistic temperature profiles.

In this study, the researchers adapted the Bayesian framework to perform the calibration, which optimised unknown material parameters to match ILLI-THERM's output and temperature measurements in the JFK section (Kennedy and O'Hagan 2001). After calibration, posterior distributions for each parameter provided insights about the significance of the input parameters. The adaptive Metropolis algorithm, an adaptive Monte Carlo Markov chain, was used to select samples to approximate the posterior distributions (Haario *et al.* 2001). In total, 309 samples were accepted from 5000 simulations. The calibration improved the performance of ILLI-THERM by reducing the root mean square error by 15%.

Calculated temperature profiles from the 5263-measured hrs covered a wide range of temperature average, temperature gradient – the difference in temperature between top and bottom of a slab – and temperature nonlinearity. The average temperature and the mean of temperatures across the slab's depth for every hour varied between 2.5°C and 30°C, while the temperature gradients covered magnitudes between −12°C and 11°C. The nonlinear area parameter, on the other hand, quantified the temperature profile's nonlinearity and varied between −2.1°C×m and 1.4°C×m (Hiller and Roesler 2010). The temperature was applied at various points through the slab section. Each point was separated by 25 mm, which allows an accurate representation of the nonlinear temperature profile.

Model validation

The research team was able to validate the FEM using comparisons between the measured and predicted strains at the bottom of the slab. This entailed reading the measured strains using JFK's instrumented airfield rigid pavement over two testing periods, April and May 2011 (Garg *et al.* 2013). The four readings were obtained from strain gauges located close to each corner of the slab – 1.5 m from the longitudinal joints and 0.25 m from the transverse.

Each slab's predicted values resulted from the FEM subjected to the calculated hourly temperature profiles. The researchers simulated three conditions, including condition 1 (C1), where the joints were free to displace and rotate; condition 2 (C2), where the joints were free to rotate – the exception being displacement in the vertical direction causing partial restraint; and condition 3 (C3), which provides partial restriction to vertical displacement and rotation along the joints. Partial restriction refers to an intermediate condition in which the edge of the slab is neither fully free nor completely restrained to rotate/displace.

Figure 2 compares the measurements and predictions for both testing periods. The validation responses were not sensitive to edge condition; however, as will be shown below, critical tensile stress and deflection were affected by the boundary conditions. The root mean square error varied between 10.3 and 14.4 microstrains, which corresponds to a variation of 3.8 and 5.2% from the average measurement, respectively. Multiple factors may contribute to the discrepancy between measured and calculated values and affect the developed model. These factors include strain gauge misalignment during construction, lack of initial slab curling data, and strain gauge bonding with the surrounding.

Figure 2. Comparison between measured and calculated corner strain at the bottom of the slab.

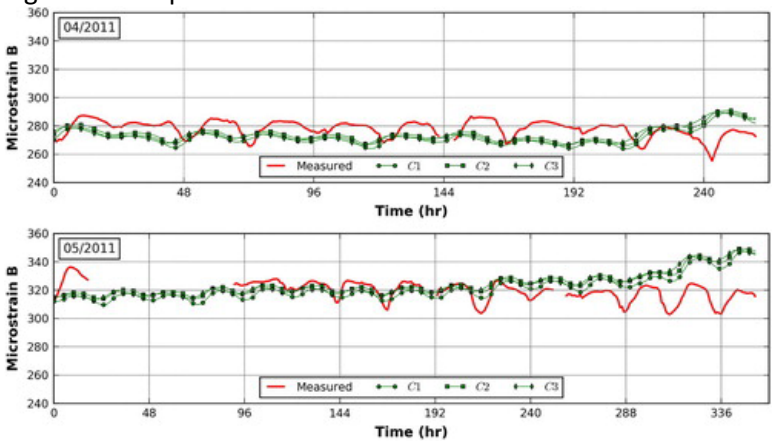

After validation, temperature profiles were analysed using FEM for seven additional testing periods – January through April, July, August, and December 2012. A total of 5263 h of temperature variations were modelled, and hourly critical tensile stress and deflection were also analysed. The impact of considering free joints in lieu of restrained joints was quantified by comparing the critical tensile stress and critical deflection at each temperature profile. For both cases, clouds of points in cartesian coordinates with the response corresponding to free joints in the horizontal axis were created – the farther the cloud of points from the equality line, the greater the effect of joint restriction is. In addition, the relevance of edge rotation restriction, during each testing period, highlights a frequency distribution in the ratio between conditions 2 and 3.

Critical tensile stresses

C*ritical tensile stress* is the highest tensile stress for all the sections points of the shell elements in the concrete slab at a specific hour. Figure 3 shows the variation of the critical tensile stress for conditions C2 and C3 with respect to C1 ($\sigma_{c,C1}$, σc, $\sigma_{c,C2}$, and $\sigma_{c,C3}$, respectively). The solid line represents cases where tensile stresses are equal to the critical stresses of C1, while points above the equality line are higher than C1.

Figure 3. Variation of critical tensile stresses for conditions 2 and 3 with respect to condition 1.

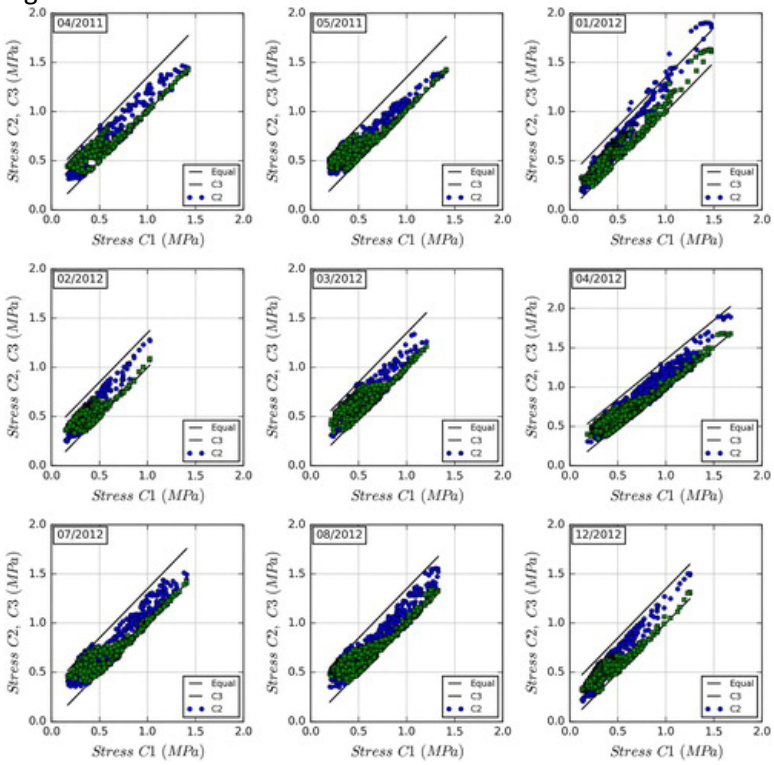

Assuming free boundaries along the joints did not result in a conservative analysis, as demonstrated by the cloud of points above the equality line. The free assumption provided the lowest tensile stresses among the three conditions. No stress ratio, with respect to C1C1 was lower than 0.94, which occurred in July 2012. The cloud of points also shows a value for the stress in C1 around 0.7 MPa from which there was no significant difference between $\sigma_{c,C1}$ and $\sigma_{c,C2}$. For instance, in May 2011, the average stress ratio between $\sigma_{c,C2}$ and $\sigma_{c,C1}$ was 1.02, when the stress was higher than 0.7 MPa. When $\sigma_{c,C1}$ was lower than 0.7 MPa, the average ratio was 1.55. The other testing periods displayed similar behaviour, where the average stress ratio for $\sigma_{c,C1}$ >0.7 MPa varied from 1.01 to 1.08, and for $\sigma_{c,C1}$ ><0.7 MPa it varied between 1.33 and 1.62.

Consequently, for this pavement structure, the calculated stresses assuming free condition and partial restriction to vertical displacement are equivalent if $\sigma_{c,C1}$ is less than 0.7 MPa. The cloud of points in Figure 3 also shows stresses enclosed between two lines with one being the equality line and the other the equality line plus 0.35 MPa. Thus, adding 0.35 MPa to the critical stress, assuming free edges, results in a conservative estimation of critical tensile stresses for the studied pavement with partially restrained edges.

The stress range was always higher for C3 than C2. The largest range of stresses observed for the testing period with the lowest temperatures occurred in January 2012. During that period, the stress range for $\sigma_{c,C3}$ was 1.72 MPa while for $\sigma_{c,C2}$ it was 1.39. This behaviour is caused by additional restraint to rotation in C3, which creates more stresses during temperature changes.

Figure 4 presents the distribution of the ratios of critical tensile stresses between $\sigma_{c,C3}$and $\sigma_{c,C2}$. The only difference between the two conditions is the partial restriction to rotation in C3. The rotational restriction's relevance increases as the ratio departs from 1. The horizontal axis indicates ranges for the tensile-stress ratio, and the vertical axis is the percentage of events that occur when the ratio falls in the corresponding range. For

instance, in December 2012, the second bar indicates that the ratio of the critical stresses varied between 0.65 and 0.75 in 6.5% of the hours measured.

Figure 4. Distribution of ratio between critical tensile stresses for C3 with respect to C2.

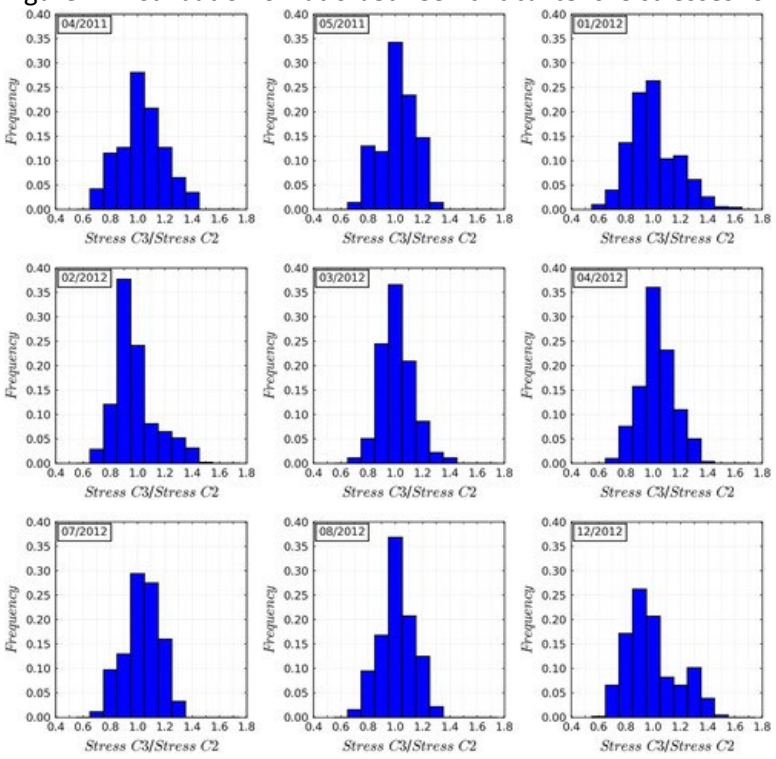

It appears the restraint to rotation along the slab joints significantly affects the critical tensile stresses. The percentage of events with ratios having small impacts, such as between 0.95 and 1.05, varied between 20.7% and 36.5% for December and March 2012, respectively. In all other testing periods, however, the ratio was larger than 1.05 or lower than 0.95 in 70% of the cases.

Temperature also influenced the impact of rotational restraint. The percentage of events when $\sigma_{c,C3}$is lower than $\sigma_{c,C2}$ is higher for colder temperatures. In January 2012, 42.6% of the events showed ratios lower than 0.95. Similarly, the percentage of events with ratios lower than 0.95 was 52.7 and 50.0% in February and December 2012, respectively. For the same two periods, the ratio $\sigma_{c,C3}/\sigma_{c,C2}$ was higher than 1.05 in 23.1 and 29.2% of the cases. For all the other testing periods, the exact opposite occurred with the highest difference happening in July 2012, when 46.6% of the events had ratios larger than 1.05 and 23.8% of them had ratios lower than 0.95.

December 2012 provided the highest percentage of cases with a difference of more than 25%. Here, the ratio $\sigma_{c,C3}/\sigma_{c,C2}$ was higher than 1.25 in 23.8% of the cases and lower than 0.75 in 14.5% of them. The large difference between C2 and C3's critical stresses, however, is not associated with the low temperature. January and February 2012s low temperatures did not have ratios above 1.25 and below 0.75 as they were not as significant of those in December 2012. This agrees with the fact that the main deformation mechanism of a slab is bending, which is manifested along the slab edges as a rotation. If edge rotation is constrained, the bending would be smaller, and vertical deflection less.

Critical deflection

Critical deflection, relevant for faulting analysis, was defined as the difference between deformed coordinates at the corner and centre of the slab with respect to the initial configuration of the corresponding testing period. In this study, only values with positive curvature were analysed because they contribute to faulting. This agrees with the transfer function used by AASHTOWare Pavement ME Design for highway pavement, which only considered corner upward deflections in faulting calculations (AASHTO 2020). The variation of the critical deflection for conditions C2 and C3, with respect to C1, is presented in Figure 5. The solid black line represents the critical deflection when no restriction exists in the vertical displacement and rotation (δ_{c1}) (i.e. equality line). Green squares correspond to points when the slab edges are partially restrained to vertical displacement (δ_{c2}), and blue circles denote critical deflection when both the vertical displacement and rotation are partially restrained (δ_{c3}).

Figure 5. Variation of critical deflection for conditions 2 and 3 with respect to condition 1.

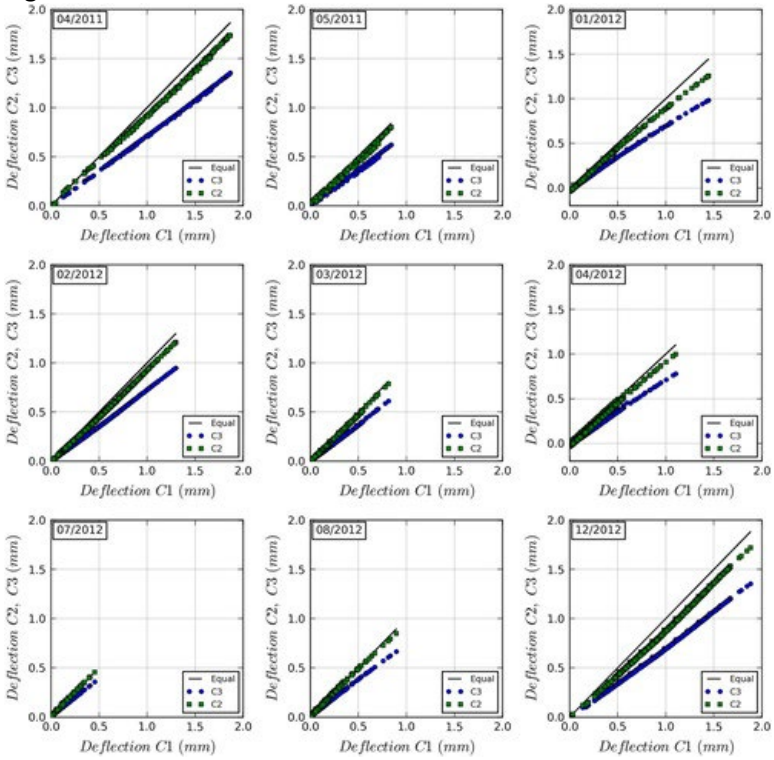

The difference between C1 and C2 is smaller than that of C1 and C3. This indicates that rotational restriction's role in faulting is more relevant than its part in vertical displacement. Linear regression's difference in slope pertaining to the cloud of points quantifies such relevance. The average slope for all testing periods for C2 and C3 was 0.944 and 0.738, respectively. Thus, restriction to displacement causes 20% of the difference between the most restrained scenario and the free condition, while the other 80% is caused by the partial restriction to rotation.

Summer months led to a higher deflection in C2 than C1. For the July and August 2012 testing periods, δ_{c2} was higher than δ_{c1} in 95% and 62% of the cases, respectively. Critical deflection is defined as the difference between deformed coordinates of the slab's corner and centre; hence, a larger critical deflection may not translate into a large deformation. δ_{c3} was seldomly greater than δ_{c1}. The highest percentage of events where the slab was partially restrained to vertical deflection and rotation provided greater faulting deflections, 7.5% during July 2012.

Summary and conclusions

The airfield rigid pavement's validated FEM showed the relevance of slab joints' rotation on critical curling stresses and deflections. Validation included strain measurements from the JFK during April and May 2011. Thermocouple reading and the enhanced integrated climate model were used to calculate temperature profiles for 5263 hrs. Three joint conditions quantified the impact of the restriction to rotation. The results revealed that joint rotation affects the critical curling stresses and deflections. In the case of critical curling stresses, partially restraining joint rotation resulted in a significant difference in 70% of the cases. As for the critical deflection, 80% of the difference between the free condition and the most restrained case was caused by the partial rotational restraint, while 20% was caused by the partial restriction to vertical displacement. Thus, calculations assuming free joints may provide initial estimation of critical curling responses for other joint conditions. In summary, joint rotation significantly affects both stresses and deflections caused by temperature. Hence, this study recommends that joint rotation be included in the long-term performance analysis of airfield rigid pavement.

Acknowledgments

The authors would like to acknowledge the financial support provided by the Federal Aviation Administration (FAA), especially the technical assistance of Navneet Garg, FAA's National Airport Pavement & Materials Research Center program manager. The assistance of Erman Gungor in calculating the temperature profiles is also acknowledged. This project was conducted in cooperation with the Illinois Center for Transportation (ICT). The contents of this paper reflect the view of the authors, who are responsible for the facts and the accuracy of the data presented herein. The contents do not necessarily reflect the official views or policies of ICT or the FAA. This paper does not constitute a standard, specification, or regulation.

Disclosure statement

No potential conflict of interest was reported by the author(s).

Additional information

Funding

This work was supported by Federal Aviation Administration.

References

AASHTO, 2020. *Mechanistic-empirical pavement design guide – a manual of practice*. Washington, D.C.: American Association of State Highway and Transportation Officials.

Asbahan, R.E. and Vandenbossche, J.M., 2011. Effects of temperature and moisture gradients on slab deformation for jointed plain concrete pavements. *Journal of Transportation Engineering*, 137 (8), 563–570. doi: 10.1061/(ASCE)TE.1943-5436.0000237

Ceylan, H., *et al.*, 2016. *Impact of curling and warping on concrete pavement. program for sustainable pavement engineering and research*. Ames, IA: Institute for Transportation, Iowa State University.

Garg, N., *et al.*, 2013. FAA's instrumentation project at John F. Kennedy International Airport to study load and environment induced responses in concrete pavements. In: *Presented at ninth international conference on the bearing capacity of roads, railways and airfields*.

Haario, H., Saksman, E., and Tamminen, J., 2001. An adaptive metropolis algorithm. *Bernoulli*, 7 (2), 223–242. doi: 10.2307/3318737

Hernandez, J. and Al-Qadi, I., 2018. Concrete pavement blowup considering generalized boundary conditions. *Journal of Transportation Engineering, Part B: Pavements*, 144 (3), 04018038. doi: 10.1061/JPEODX.0000072

Hernandez, J. and Al-Qadi, I. L., 2019. Closed-form solution for curling responses in rigid pavements. *Journal of Engineering Mechanics*, 145 (2), 04018133. doi: 10.1061/(ASCE)EM.1943-7889.0001563

Hiller, J.E. and Roesler, J.R., 2010. Simplified nonlinear temperature curling analysis for jointed concrete pavements. *Journal of Transportation Engineering*, 136 (7), 654–663. doi: 10.1061/(ASCE)TE.1943-5436.0000130

Huang, Y. H., 2004. *Pavement analysis and design*. 2nd ed. Upper Saddle River, NJ: Pearson Prentice Hall.

Ioannides, A.M. and Khazanovich, L., 1998. Nonlinear temperature effects on multilayered concrete pavements. *Journal of Transportation Engineering*, 124 (2), 128–136. doi: 10.1061/(ASCE)0733-947X(1998)124:2(128)

Kennedy, M.C. and O'Hagan, A., 2001. Bayesian calibration of computer models. *Journal of the Royal Statistical Society: Series B (Statistical Methodology)*, 63 (3), 425–464. doi: 10.1111/1467-9868.00294

Lytton, R.L., *et al.*, 1993. An integrated model of the climatic effects on pavements.

Mohamed, A. and Hansen, W., 1997. Effect of nonlinear temperature gradient on curling stress in concrete pavements. *Transportation Research Record: Journal of the Transportation Research Board*, 1568, 65–71. doi: 10.3141/1568-08

Nishizawa, T., *et al.*, 1996. Curling stress equation for transverse joint edge of a concrete pavement slab based on finite-element method analysis. *Transportation Research Record: Journal of the Transportation Research Board*, 1525, 35–43. doi: 10.1177/0361198196152500105

Richardson, J.M. and Armaghani, J.M., 1987. Stress caused by temperature gradient in Portland cement concrete pavements. *Transportation Research Record: Journal of the Transportation Research Board*, 1121, 7–12.

Sen, S. and Roesler, J., 2018. Contextual heat Island assessment for pavement preservation. *International Journal of Pavement Engineering*, 19 (10), 865–873. doi: 10.1080/10298436.2016.1213842

Shoukry, S.N., *et al.*, 2007. Validation of 3DFE analysis of rigid pavement dynamic response to moving traffic and nonlinear temperature gradient effects. *International Journal of Geomechanics*, 7 (1), 16–24. doi: 10.1061/(ASCE)1532-3641(2007)7:1(16)

Solaimanian, M. and Kennedy, T.W., 1993. Predicting maximum pavement surface temperature using maximum air temperature and hourly solar radiation. *Transportation Research Record, Journal of the Transportation Research Board*, 1417, 1–11.

Westergaard, H., 1927. Analysis of stresses in concrete pavements due to variations of temperature. *Highway Research Board Proceedings*, 6, 201–215.

William, G.W. and Shoukry, S.N., 2001. 3D finite element analysis of temperature-induced stresses in dowel jointed concrete pavements. *International Journal of Geomechanics*, 1 (3), 291–307. doi: 10.1061/(ASCE)1532-3641(2001)1:3(291)

Yoo, P.J., *et al.*, 2006. Flexible pavement responses to different loading amplitudes considering layer interface condition and lateral shear forces. *The International Journal of Pavement Engineering*, 7 (1), 73–86. doi: 10.1080/10298430500516074